ACDIS
Research
Report

Climate Action Game Experiment Motivation and Role of Radiative Forcing

Chenghao Ding
Department of Nuclear, Plasma, and Radiological Engineering
University of Illinois at Urbana-Champaign

Clifford E. Singer
Program in Arms Control & Domestic and International Security
University of Illinois at Urbana-Champaign

Research of the Program in Arms Control
& Domestic and International Security

University of Illinois at Urbana–Champaign

July 2022

The research for this publication is supported by the University of Illinois. It is produced by the Program in Arms Control & Domestic and International Security at the University of Illinois at Urbana-Champaign.

ACDIS Publication Series: ACDIS *Swords and Ploughshares* is a periodic journal of collected articles aimed at a general audience. The ACDIS *Occasional Paper* series is the program's principal publication for circulating the scholarly analytical results of faculty, students, and visiting researchers associated with ACDIS. The ACDIS *International Security Policy Brief* series highlights ongoing academic research at ACDIS and the University of Illinois that serves to inform U.S. and international policy decisions. The ACDIS *Research Reports* series publishes technical reports and the findings from contracted grant research. For additional information and to download publications, visit the ACDIS home page at: http://acdis.illinois.edu/

Published 2022 by ACDIS//ACDIS DIN:1.2022

University of Illinois at Urbana–Champaign 359 Armory Building, 505 E. Armory Ave.
Champaign, IL 61820-6237

Series Editor: Jazmin Tejeda

Climate Action Game Experiment Motivation and Role of Radiative Forcing

CHENGHAO DING
Department of Nuclear, Plasma, and Radiological Engineering
University of Illinois at Urbana Champaign

CLIFFORD E. SINGER
csinger@illinois.edu
Program in Arms Control & Domestic and International Security
University of Illinois at Urbana Champaign

Abstract. This report is the first of a series that examines a set of questions about the relationship between policy decisions and the future of climate change. These questions are framed quantitatively by results from a data-driven analysis tool called the Climate Action Gaming Experiment (CAGE). Descriptions of results using a previous version of CAGE provide examples [1, 2]. Motivations for developing CAGE include education, research, and potential support for development of public policy. CAGE differs from many other simple and intermediate complexity integrated assessment tools in its emphasis on including a framework for human participant experiments relevant to all three of these motivations.

1. Motivations for CAGE

From an educational perspective, the CAGE software and its documentation are designed for use by a mix of people with and without primarily backgrounds in STEM (science, technology, engineering and mathematics). CAGE provides this mix of people with an opportunity to get real-time feedback on physical and economic consequences during simulated international interactions involving development of policies relevant to climate change.

From a research perspective, a goal of work with CAGE is developing probability distributions for a real-world outcome, with inclusion of experimental results on how people react to information about expected outcomes from climate change. That information includes (1) physical consequences, (2) impacts on regional economic productivity, and (3) implications of changes in productivity for human welfare. A motivation for this approach is the idea that computational results are necessary but not sufficient components of an analysis of the complex mix of social and psychological factors that influence decision making relevant to climate change.

There are two policymaking contexts where CAGE results could be helpful. First, many groups of people have to plan for consequences of climate change but have a very small influence on the overall outcome. Such people need input not only on the consequences of different outcomes, but also an analysis of how likely various possible outcomes are. Second, even people with the most influence on climate policy can reasonably expect that their efforts as individuals or in small coherent groups will lead to only a small change in the overall outcome. A starting point for development of climate-relevant policy is data-informed insight into what outcomes are likely even without implementation of a policy change being considered. There is, of course, a large gap between practicable simulation experiments and the actual process of policy development and implementation. A purpose of this series of reports is to provide an example of a start on bridging that gap. A starting point for making this series of reports publicly available includes posting of these [3]:

1. Climate Action Game Experiment Motivation and Role of Radiative Forcing (this report)
2. Calibration and Extrapolation of a Simple Global Carbon Balance Model
3. Non-anthropogenic Influences on Global Average Temperature
4. Global Heat Balance Model Calibration
5. Extrapolations of Global Average Temperature, Sea Level Rise, and Ocean pH Change
6. Global Heat Balance Equation Probability Distribution and Extrapolations

These reports are designed both for reading by an interdisciplinary audience and by researchers who may want more detailed descriptions of the mathematical analysis methods used. So, where feasible, the main text of each report is designed to be accessible to a broader audience while more technical details are covered in appendices.

The above-mentioned six reports provide background that can support updating previous work [4] on climate change impacts on economic productivity. Those impacts include both direct effects of changes in the atmospheric carbon dioxide concentration ($<CO_2>$) on agriculture, forestry, human cognition, and coral reefs and indirect effects via changes in the global heat balance. The CAGE framework allows for policies that change the evolution of $<CO_2>$, interacting with extrapolations of other historical anthropogenic contributions to radiative forcing. It also allows for examination of some of the consequences of solar radiation management (SRM) via historically unprecedented deliberate changes in short-lived climate forcing, e.g. by high-altitude injection of sulfur to create stratospheric haze. Developing insight into the probability of implementation of broad enough global cooperation on limiting increases in previous types of anthropogenic radiative forcing to avoid otherwise adversely affected regions resorting to such unprecedented SRM is something that CAGE is designed for.

Extrapolations of radiative forcing that are calibrated against historical data play a central role in the CAGE framework. This report describes the methods used for anthropogenic radiative forcing other than that from $<CO_2>$. Drawing on results from the recent Zero Emissions Commitment Model Inter-comparison Project [5], the next report describes calibration and extrapolation of the global carbon balance model used in CAGE. The third report provides complementary information on non-anthropogenic influences on global average temperature. Those include volcanoes, changes in incoming solar irradiance, and the El Niño Southern Oscillation (ENSO). The three subsequent reports focus on the history and future of the global heat balance.

2. Global Heat Balance

Contributions to radiative forcing are drivers to changes, here referred to as τ, in annually and globally geographically averaged temperature. The historically observed evolution of τ is be approximated using the equation

$$c_{th}\tau' = F - \tau/\beta \tag{2.1}$$

Here, τ' is the rate of change in °C/yr of τ. The units of radiative forcing F are watts per square meter (W/m^2). F is the annually averaged global watts of increase over a reference year (1750 for CAGE, with total solar irradiance approximated as its 1749–1755 average), divided by the surface area of the earth. In CAGE, F includes both small changes in solar energy input and anthropogenically driven changes in radiative forcing compared the reference year. In a steady state, the rate of change τ' of τ would be zero, and then τ would equal βF. For CAGE, the reference year is approximated as being in steady state. Since F is the change in radiative forcing from the reference year, in that year $F = 0$ and thus also $\tau = 0$, which is the initial condition for equation (2.1).

The units of β are °C/(W/m^2). The larger β is, the higher the temperature increase in equilibrium for a given level of F. Here, β is called the climate sensitivity. This is not to be confused with what is commonly called the equilibrium climate sensitivity (ECS), which has units of °C. What is commonly called equilibrium climate sensitivity is the increase in global average temperature after $<CO_2>$ is increased two-fold over a specified base level and then held constant, ideally with no other changes in radiative forcing. Approximating radiative forcing from $<CO_2>$ as $\alpha \ln(<CO_2>/C_0)$ with α=5.35 w/m^2 and C_0=278 parts per million by volume (ppm) [6], the relationship between ECS and β is ECS=$(\alpha \ln 2)\beta = 3.7\beta$.

However, it should be kept in mind that ECS estimates are often reported in the context of results from comprehensive earth systems models (ESMs) that differ in many important respects

from a simpler global heat balance calculation. In particular, the computed effects on global average temperature from tropospheric aerosols in ESMs can be the result of complex regionally and seasonally dependent atmospheric chemistry and molecular and radiative transport analyses. If so, global and annually averaged radiative forcing from tropospheric aerosols is an output from such calculations, not an input to them. It is thus not to be expected that the value of β resulting from using such estimates of tropospheric aerosol shielding as a contribution to radiative forcing in equation (2.1) will lead to an estimate of β that corresponds to ECS/3.7 estimates from the more comprehensive ESMs.

How quickly τ responds to changes in radiative forcing in equation (2.1) is determined by the parameter c_{th}. For slow changes in F on timescales of several decades, the heating effect of increasing radiative forcing is felt hundreds of meters deep in the oceans. For rapid changes in forcing like the cooling from the 1991 Mount Pinatubo volcanic eruption, there is primarily more near-surface transient cooling, which in turn reduces radiative losses. For changes that are small compared to the difference T_{abs} between the earth's surface temperature and the coldest temperature found anywhere in the universe, that change in radiative losses can be approximated as proportional to the temperature change. As a result, the change in radiative loss following a short transient in radiative forcing quickly nearly balances that change in radiative forcing. That leads to only a transient observable effect on global average temperature for Mount Pinatubo, which produced an estimated larger change in radiative forcing than observed to date from other volcanoes in the twentieth and twenty-first centuries [7].

Here, c_{th} is called the thermal inertia parameter. The product βc_{th}, which has units of years, is referred to as the thermal inertia timescale. With a constant value of c_{th}, equation (2.1) is only designed to be used for changes in radiative forcing on timescales of a few decades. Transient changes due to large volcanic eruptions and short-term variations in solar irradiance are handled separately, as described in the third report in this series.

With a constant value of c_{th} designed for radiative forcing changes on a timescale of a few decades, solutions of equation (2.1) can be expected to produce a more rapid approach to an eventual equilibrium temperature than a more complete treatment of thermal energy transport, if the radiative forcing approaches a limit value very slowly. For the kind of economic impact analysis that CAGE is designed for [4], however, timescales much longer than an economic discounting timescale of at most a few decades are not of particular interest.

The approximation of a linear response of τ to changes in total radiative forcing has been widely used [8] but has its limitations for large values of τ. At the minimum, omitted from the linear equation are nonlinear corrections to radiative losses of order τ/T_{abs}, where $T_{abs} \sim 290$ in round numbers. That nonlinear correction is small due to the $(\tau + T_{abs})^4$ dependence of radiative losses on temperature. Neglecting these particular nonlinear corrections leads to errors only of about one percent for increases in τ of up to 2.6°C. Other nonlinear responses may be larger. However, the sign of the coefficient of a term quadratic in τ in the global heat balance equation is uncertain. Limits on the absolute value of the nonlinear term [9] for values of τ up to 2.6°C suggest that its effect is at most comparable to other uncertainties in radiative forcing ([10], figure 7.6, p. 7-182). The CAGE formulation is designed only for extrapolations up to values of τ for which nonlinear corrections equation to the global heat balance equation are not essential. That is to say for global warming only up to the point where a response such as stratospheric sulfur injection might serve as a last resort to keep global warming from otherwise reaching a "tipping point" with a strongly nonlinear response to radiative forcing.

3. Components of Radiative Forcing

The contribution of the Intergovernmental Panel on Climate Change (IPCC) Working Group 1 to the IPCC Sixth Assessment Report (hereinafter AR6) provides an update on ten contributions to

anthropogenic radiative forcing in addition to <CO_2> [10]. Those ten are considered here in three groups. In the third group, sums for related sources are used.

1. (a) <N_2O>, (b) <CH_4>, (c) stratospheric water vapor
2. (a) halogens, (b) contrails, (c) land use changes
3. (a) stratospheric and tropospheric ozone and black carbon on snow, (b) tropospheric aerosols

3.1. **Nitrous Oxide and Methane.** The first group of contributions to radiative forcing includes contributions from increases over Julian year 1750 in values of the atmospheric concentrations <N_2O> and <CH_4>. Fits to data and extrapolations are shown for <N_2O> in Figure 1a and for <CH_4> in Figure 1b. The fits to the atmospheric concentration measurements are solutions of equations of the form

$$G' = S - (G - G_0)/t_G \tag{3.1}$$

Here G is atmospheric concentration in parts per billion by volume (ppb) and G' is the annual rate of change of G. The atmospheric lifetimes t_G of <CH_4> and <N_2O> that are used here are respectively 9.1 and 116 years (AR6 p. 5-34 and p. 5-47). The emission rate in ppb/yr is $S = a_1(u - u_0)$. Here

$$u = 1/(1 + e^{-x}) \tag{3.2}$$

is the unit logistic function and $x = (t - a_2)/a_3$. The initial value of u is $u_0 = 1/(1 + e^{-x_0})$ with $x_0 = (t_0 - a_2)/a_3$ and t_0 the initial time when $G = G_0$. Thus, anthropogenic emissions start at 0 at time t_0. The long-term limit of the emission rate $a_1(1 - u_0)$ is close to the value of the fitting parameter a_1, since the values of u_0 are small. The fitting parameter a_2 is the time, called the inflection time, at which $x = 0$ and $u = 1/2$. The fitting parameter a_3 is the inverse of the rate of exponential decay of the difference $1 - u$ as $u \to 1$ in the long-term limit. Logistic functions are used extensively in this report for quantities that initially grow approximately exponentially but are subject to limits on growth that preclude reaching arbitrarily large values.

The parameters, a_1, a_2, a_3, and initial atmospheric concentrations G_0 listed in Table 1 were estimated by minimizing the sum of the squares of the differences between solutions of equation (2.1) for G and the data points shown in Figures 1a and 1b for <N_2O> and <CH_4> respectively. Given these parameters, moving the solution of equation (3.1) forward can be done as described below in section A.7.

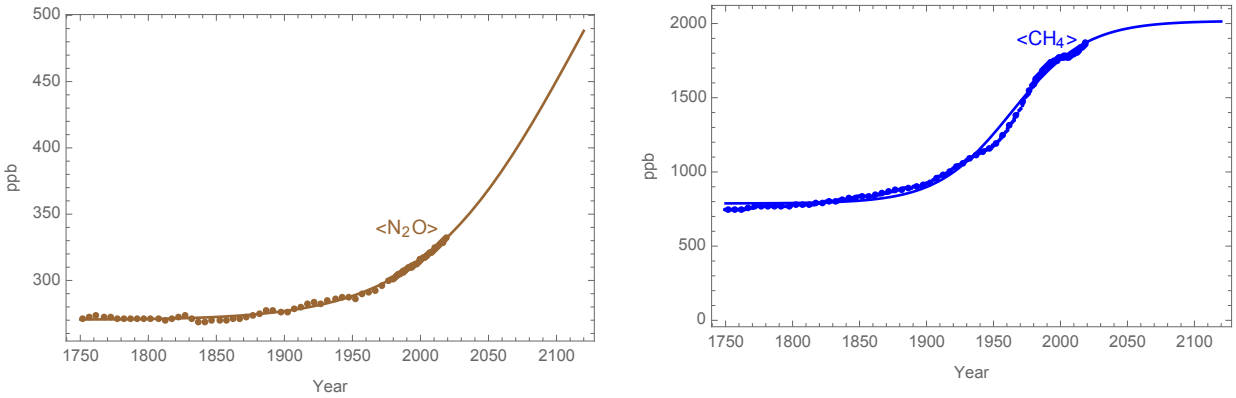

Figure 1. Data (dots) and extrapolated fits to atmospheric concentrations of (a) nitrous oxide and (b) methane.

Equation 3.1 is solved starting with a value of G of $G_1 = G_0$ for Julian year 1750. Following eighteenth century polymath Leonard Euler, a simple way of doing this is to approximate G' as

$G_i - G_{i-i}$ to get

$$G_i = G_{i-1} + S_{i-1} - (G_{i-1} - G_0)/t_G \tag{3.3}$$

for integers $i > 0$, where $S_i = 1/(1 + e^{-x_i}) - 1/(1 + e^{-x_0})$ and $x_i = (1750 + i - a_2)/a_3$. Then successively compute G_i for as many years subsequent to 1750 as desired. A comparison of the accuracy of this method to a solution treating G as a continuous function of time as used here is described in Section A.7.

Table 1. N_2O, CH_4 and Stratospheric H_2O Constants

	G_0	a_1	a_2	a_3
Parameter Units:	ppb	ppb/yr	Julian Year	years
N_2O Emissions Equation	270.6	4.95	2059.82	50.76
CH_4 Emissions Equation	788.2	135.21	1954.45	27.03
t_G and a_H	G=N_2O	G=CH_4	a_H	(W/m^2)/ppb
	9.1 yr	116 yr	0.000048	

Figure 2a shows radiative forcing from <N_2O> and <CH_4>, calculated using formulas in section A.6. Oxidation of methane also produces radiative forcing via an increase in stratospheric water vapor. So, the sum of anthropogenic radiative forcing from <CH_4> and forcing from a related increase stratospheric water vapor is also shown in figure 2a. The forcing from stratospheric water water is 0.000048 W/m^2 per ppb of the increase in <CH_4> over its value in 1750. That proportionality in a given year is to what the value of <CH_4> was two years earlier [11].

3.2. **Logistic Functions in Fits to Radiative Forcing.** The second group listed above includes volatile compounds containing the halogens chlorine and/or fluorine, contrails and cirrus cloud changes related to aviation, and land use changes that affect the earth's albedo. The evolution of radiative forcing from each of these is fit with a constant plus a logistic function, i.e. $b_0 + b_1 u = b_0 + b_1/(1 + e^{-x})$, with $x = (t - b_2)/b_3$.

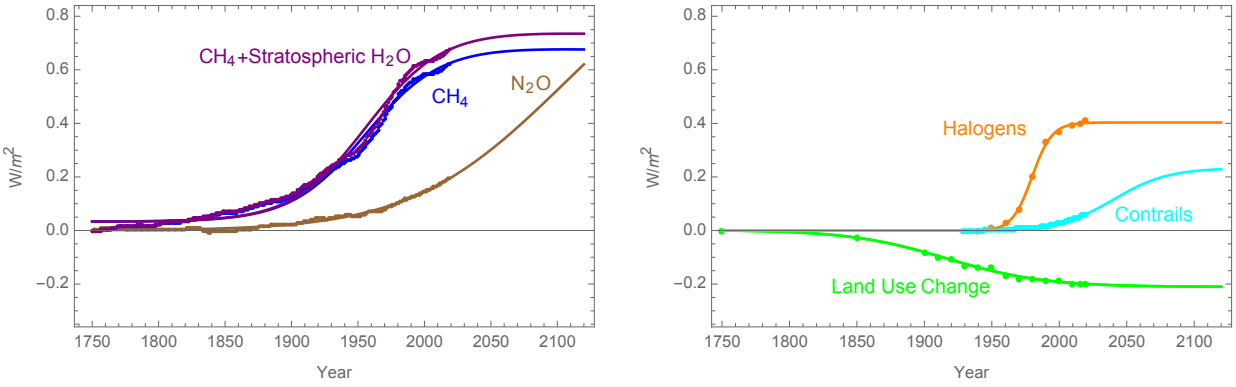

Figure 2. (a) Extrapolations of fits to anthropogenic radiative forcing from nitrous oxide, methane, and from methane and stratospheric water vapor combined. (b) Data (dots) and fits to anthropogenic radiative forcing from halogens, from contrails and cirrus clouds, and from land use changes.

Figure 2b shows least squares fits to historical data and extrapolations of functions of the form $b_0 + b_1 u$ to radiative forcing from gases that contain chlorine and/or fluorine (halogens). Figure 2b

also shows historical data and extrapolations from the interaction between aviation-related contrails and cirrus clouds changes, and from land use changes. These data entries are for the change in radiative forcing from its 1750 value. The constants b_0 in the expression $b_0 + b_1 u$ are constrained to have the radiative forcing be zero for Julian year 1750 for land use changes. The constants b_0 for contrails and halogens are constrained to have the radiative forcing be zero in 1927 and 1940 respectively. Those are the last years with zero forcing in the respective input data streams.

3.3. **Tropospheric Aerosols, Ozone, and Black Carbon on Snow and Ice.** The third group of contributions to radiative forcing listed above includes short-lived and thus regionally localized atmospheric pollutants. Tropospheric and stratospheric ozone combined produce a net positive radiative forcing, as does black carbon on snow. (The term black carbon on snow is a shorthand for the combination of black carbon on snow and black carbon on ice.) Tropospheric aerosols produce a negative radiative forcing (i.e. radiative shielding). Radiative forcing from tropospheric aerosols includes both direct interactions of aerosols with radiation and effects of the aerosols on clouds. These are all connected to sources of regional pollution. Those connections provide incentives to reduce emissions in source countries as those countries feel the effects of that pollution and implement measures to limit or reduce them. The absolute values of the estimated radiative forcing from these have historically grown and then either nearly reached a maximum and may be on the way towards declining (in the case of ozone and black carbon on snow) or already have started to decline (in the case of tropospheric aerosols).

Table 2 lists the fitting functions and parameters used for members of the second and third groups of contributions to radiative forcing. These formulas apply from 1750 on. They give forcing values of 0 in 1750 for land use changes, for ozone plus black carbon on snow and ice, and for tropospheric aerosols. They give 0 for contrail/cirrus-cloud effects through 1927 and for halogens through 1940. For the three functions with time-varying contributions proportional to u, the absolute value of radiative forcing approaches a maximum of $|b_0 + b_1|$ in the long-term limit. The function $u(1-u)$ is proportional to the temporal rate of change of u. For the two functions with a time-varying term proportional to $u(1-u)$, the absolute value of radiative forcing reaches a maximum of $|b_0 + b_1/4|$ at time $t = b_2$.

Table 2. Constants and Logistic Function $u = 1/(1 + e^{-(t-b_2)/b_3})$ Parameters

Type	Formula	b_0	b_1	b_2	b_3
	Units:	W/m^2	W/m^2	Julian Year	years
Land use change	$b_0 + b_1 u$	0.002	-0.213	1916.49	35.96
Contrails-cirrus	Max[0,$b_0 + b_1 u$]	-0.002	0.234	2040.36	20.15
Halogens	Max[0,$b_0 + b_1 u$]	-0.002	0.405	1979.83	7.41
Ozone +BC on snow	$b_0 + b_1 u(1-u)$	-0.002	2.383	2041.44	42.99
Tropospheric aerosols	$b_0 + b_1 u(1-u)$	0.002	-5.423	1994.81	32.11

Figure 3a shows least squares fits to historical data and extrapolations of the form $b_0 + b_1 u(1-u)$ for tropospheric aerosols and for the combination of ozone and black carbon on snow. Radiative forcing from black carbon on snow has a minor effect (0.08 W/m^2 in 2019) compared to the sum of tropospheric ozone forcing and stratospheric ozone shielding (totaling 0.47 W/m^2 in 2019) [10]. (Forcing from ozone and black carbon on snow are combined here, as detailed in Appendix A, because both are connected to regional pollution sources, and because the information available for black carbon is insufficient to support an extrapolation of its effect alone.) Comparing Figures 3a

and 3b indicates that the AR6 estimate of tropospheric aerosol shielding was sufficient to cause a noticeable dip in total anthropogenic radiative forcing, from other than $<CO_2>$, up to 1964.

Figure 3b also suggests that leveling off radiative forcing from $<CO_2>$ may not be sufficient to keep global average radiative forcing from increasing throughout the twenty-first century in the face of reduced tropospheric aerosol shielding. Indeed, the radiative forcing in 2100 shown in Figure 3b is 1.81 W/m^2, comparable in magnitude to estimated radiative forcing of 2.16 W/m^2 from $<CO_2>$ in 2019. As described in the next report in this series, some reduction of $<CO_2>$ would be expected to follow from an abrupt halt to anthropogenic atmospheric $<CO_2>$ emissions. Even in the unlikely event of such an abrupt change, keeping the sum of radiative forcing in 2100 from $<CO_2>$ and the sum plotted in Figure 3b to the same as in 2019 with the extrapolation shown in Figure 3b by reducing $<CO_2>$ would require a value for the latter of 0.5 W/m^2, a level not seen since 1920. That could require large scale and enduring removal of CO_2 from ambient air. Moreover, even with constant radiative forcing at 2019 levels, there would still be global heat imbalance, so the solution for τ in equation (2.1) would initially continue to rise at its year 2019 rate before eventually leveling off at a higher equilibrium value.

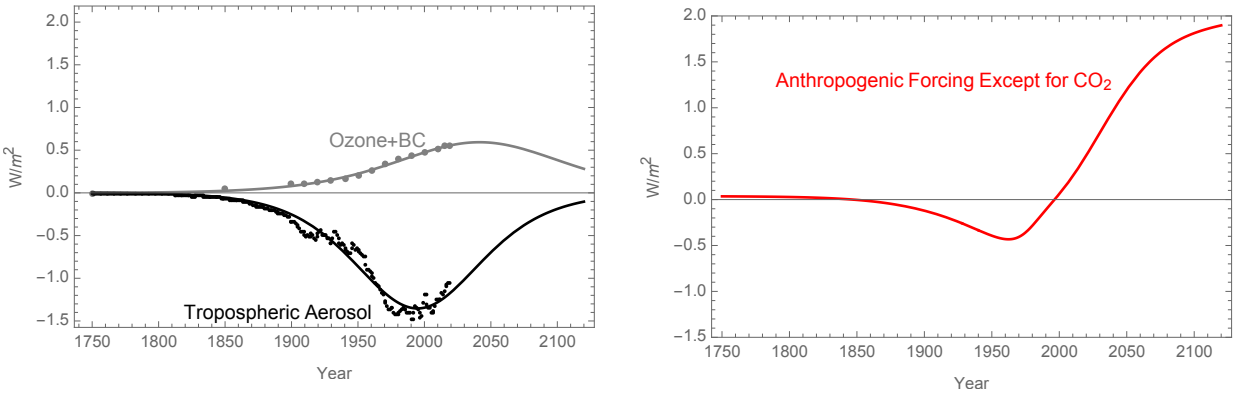

Figure 3. (a) Constant plus a dependence proportional to the time derivative of a logistic function for radiative forcing from tropospheric aerosols and from the sum of radiative forcing from ozone and black carbon on snow. (b) Sum of all anthropogenic radiative forcing except from $<CO_2>$.

These observations point out the importance of attention to the other contributions to radiative forcing shown in Figure 2. Radiative forcing from halogens might be gradually reduced by limiting emissions of those with atmospheric lifetimes of several decades. Growth of air transport could be limited in part by substitution of transportation with long-distance communication alternatives. Some reduction of atmospheric methane emissions might well accompany changes in extraction of fossil fuels resources, but a significant fraction of anthropogenic methane emission is associated with agriculture. Effecting significant changes in land use patterns and agriculture on a global basis would be a complex endeavor. The same applies to altering agricultural contributions to nitrous oxide emissions and how land use patterns impact the earth's albedo.

Appendix A. Data Management and Use

This appendix describes how the dots shown in the figures above were obtained. It also provides additional information on how the curves in those figures were obtained. As a start on this, Table 3 lists radiative forcing estimates from AR6 Annex III, Table AIII.3.

Table 3. AR6 Table AIII.3 W/m^2 and BC Modification

Year	LUC	Halogens	Ozone	Strat. H_2O	AR6 BC	BC Used
1750	0	0	0	0	0	0
1850	-0.03	0	0.03	0	**0.01**	1 %
1900	-0.08	0	0.08	0.01	**0.02**	2 %
1910	-0.10	0	0.09	0.01	0.03	2 1/3 %
1920	-0.11	0	0.10	0.02	0.03	2 2/3 %
1930	-01.3	0	0.12	0.02	**0.03**	3 %
1940	-0.14	0	0.14	0.02	0.03	3 1/3 %
1950	-0.14	0.01	0.17	0.02	0.03	3 2/3 %
1960	-0.17	0.03	0.22	0.03	**0.04**	4 %
1970	-0.18	0.08	0.28	0.03	**0.05**	5 %
1980	-0.18	0.20	0.33	0.04	0.06	6 %
1990	-0.19	0.33	. 0.36	0.04	*0.07*	6 2/3 %
2000	-0.19	0.37	0.40	0.05	*0.07*	7 1/3 %
2010	-0.20	0.39	0.44	0.05	**0.08**	8 %
2015	-0.20	0.40	0.47	0.05	**0.08**	8 %
2019	-0.20	0.41	0.47	0.05	**0.08**	8 %

A.1. **Black Carbon on Snow and Ice.** To undo some of the rounding used to produce the AR6 black carbon on snow and ice (BC) numbers, only the entries in bold and italic type in the AR6 BC column in Table 3 were used. The years 1990 and 2000 were not used, and instead the number 0.07 was assigned to year 2015. Linear interpolation of that assignment and the numbers in bold type was used to get the numbers in the column labelled BC Used.

A.2. **Nitrous Oxide, Methane, and Stratospheric Water Vapor.** Extensive time series estimates of $<N_2O>$ and $<CH_4>$ are available without relying on information from AR6, so those estimates were used to produce Figures 1a and 1b above. For $<N_2O>$ and $<CH_4>$, quinquennially spaced Law Dome ice core measurements were used for 1752–1977 [12, 13]. Those numbers were multiplied by 1.007 and 1.066 respectively to make the 1979 values match direct atmospheric concentration measurements [6].

Radiative forcing from stratospheric water vapor (Strat. H_2O), was computed using $<CH_4>$ values to estimate increases $\Delta<CH_4>$ over 1750, at times two years [11] before the years listed in Table 3. A proportionality constant $a_H = 0.000048$ W/m^2 was estimated by finding a value of a_H that minimized the sum of squares of f_H-Round$[a_H\Delta<CH_4>]$, where Round indicates rounding to the nearest 0.01. This approach matched the rounded values of $a_H\Delta<CH_4>$ to the rounded numbers reproduced in Table 3.

A.3. **Contrails.** Table AIII.3 from AR6 also lists eight estimates of radiative forcing from contrail effects, but these are also rounded to the nearest 0.01, with a maximum value of only 0.06. Instead of using these numbers, a more detailed set of estimates of contrail and cirrus cloud radiative forcing from 2000–2018 was used [14]. Those numbers are within 0.002 W/m^2 of the year 2010 and rounded 2015 AR6 Table AIII.3 values, but lower by 0.012 W/m^2 than the year 2000 AR6 Table AIII.3 number that appears to be rounded up to 0.04 W/m^2. The annual 2000–2018 estimates were linearly extrapolated to 2019 and prepended with annual AR5 [15] estimates from 1750–2099 rescaled with a multiplicative factor of 0.862. That factor is the average of the 2000–2011 portion of the 2000–2018 estimates divided by the 2000–2011 portion of the AR5 estimates. This procedure produced the dots shown above in Figure 2a.

A.4. **Tropospheric Aerosols.** For tropospheric aerosols, there was sufficient resolution on a 1750–2019 graph in figure 2.10 of AR6 to extract an annual time series for radiative forcing for those years. This was done by extracting points with an average spacing of 1 year from 1880–2019 and of 3 years from 1810–1880, linearly interpolating including a zero value in 1750, and evaluating the interpolated result annually from 1750–2019. (Repeating a similar procedure using the median plot from figure 7 of a year 2021 paper [16] did not suggest using those results as an alternative to that used to produce Figure 3a above.) The procedure used here produced the dots shown above in Figure 3a. AR6 also provides uncertainty ranges for radiative forcing estimates, with particularly striking uncertainty for tropospheric aerosols. There are also indications that the efficacy of radiative shielding from tropospheric aerosols may be lowered when in combination with radiative forcing of larger absolute value from well-mixed greenhouse gases [17]. The implications of uncertainty in the radiative forcing estimate for tropospheric aerosols are dealt with in the fourth and sixth reports in this series.

A.5. **Temporal Resolution.** The data entries in Table 3 are increasingly temporally sparse moving back in time. The earlier radiative forcing estimates are small enough to have comparatively little impact on the parameter fitting results. The earlier estimates may also have lower accuracy than for more recent years. The ice core measurements have lower temporal resolution than direct atmospheric measurements used to estimate $<N_2O>$ and $<CH_4>$. That consideration motivated also using more data points from the direct measurements than from ice cores when producing the fitting curves for $<N_2O>$ and $<CH_4>$ shown above in Figures 1a and 1b.

This approach did rely more heavily on somewhat temporally sparse estimates of several contributions to radiative forcing compared to what might be gleaned from trying independently to make comparable estimates based on available literature and online data collections. However, despite the fact that the AR6 report does not provide enough information for an investigator to independently reproduce the results in its Table AIII.3, it was decided to limit the radiative forcing estimates to those listed in that table for five of the anthropogenic contributions to radiative forcing that are used in CAGE. One reason for this is that the primary purpose of developing CAGE was to support interactive simulations of international negotiations on some aspects of policies related to climate change. For information on radiative forcing and its physical effects, the AR6 report appeared to be both the most recent and most influential source likely to help frame how such negotiations are approached. Thus, for CAGE, extensive use of AR6 based the forcing estimates listed above in Table 3 and for tropospheric aerosols as graphed above in Figure 3a seemed appropriate.

A.6. **Radiative Forcing Formulas.** The radiative forcing formulas used here (from AR6 Table 7SM-3) as functions of $N=<N_2O>$ and $M=<CH_4>$ are described in Table 5.

Table 5. Radiative Forcing Formula Constants

j	1	2	3
a_j	-2.4785×10^{-7}	-3.4197×10^{-7}	-8.9603×10^{-5}
a_j units	W m^{-2} ppm^{-2}	W m^{-2} ppm^{-1}	W m^{-2} ppb^{-1}
b_j	7.5906×10^{-4}	2.5455×10^{-4}	-1.2462×10^{-4}
b_j units	W m^{-2} ppm^{-1}	W m^{-2} ppb^{-1}	W m^{-2} ppb^{-1}
c_j	-2.1492×10^{-3}	-2.4357×10^{-4}	0
c_j units	W m^{-2} ppb$^{-1/2}$	W m^{-2} ppb^{-1}	
d_j	5.2488 W m^{-2}	0.12173 W m^{-2} ppb$^{-1/2}$	0.045194 W m^{-2} ppb$^{-1/2}$
$\{C_0, M_0, N_0\}$	277.15 ppm	731.41 ppb	273.87 ppb

Radiative forcing for <N_2O> in these formulas depends slightly on <CO_2>. For the plot in figure 2a above, <CO_2> was set to its year 2019 value of 409.8 ppm when calculating radiative forcing from <N_2O>. If a value of $C = 560$ ppm is used instead, then the nitrous oxide radiative forcing is 1.2% lower. This small difference indicates how very weak the dependence forcing from nitrous oxide is on <CO_2>. For future reference in this report series, the constants used in a formula for radiative forcing from C=<CO_2> are also listed in Table 4. The formulas are as follows. For $C_0 < C < 1808$ ppm,

$$F_C = (d_1 + a_1(C - C_0)^2 + b_1(C - C_0) + c_1\sqrt{N})\ln(C/C_0) \tag{A.1}$$

For nitrous oxide,

$$F_N = (a_2\sqrt{C} + b_2\sqrt{N} + c_2\sqrt{M} + d_2)(\sqrt{N} - \sqrt{N_0}) \tag{A.2}$$

For methane,

$$F_M = (a_3\sqrt{M} + b_3\sqrt{N} + d_3)(\sqrt{M} - \sqrt{M_0}) \tag{A.3}$$

A.7. **Greenhouse Gas Balance Equation Solution Methods.** This appendix ends with a description of solutions for the evolution of <N_2O> and <CH_4> for a constant plus logistic function evolution of anthropogenic emissions considered as continuous functions of time. For the purpose of calibrating the parameters in the expressions for emissions sources S against historical data, it is convenient to have analytic function solutions to equation (3.1). Multiplying that equation through by a_3, defining the dimensionless ratio $\delta = b_3/t_G$, and letting $H = (G - G_0)/(a_1a_3)$ gives

$$dH/dx = u - u_0 - H\delta \tag{A.4}$$

Since G is increase in atmospheric concentration since time t_0 and H is proportional to $G - G_0$, the initial condition at time t_0 is $H = 0$. The solution to equation (A.3) with that initial condition is

$$H = e^{-\delta x}(I - I_0) - (u_0/\delta)(1 - e^{-(x-x_0)\delta}) \tag{A.5}$$

Here I_0 is the value for $x = x_0$ of the integral $I = \int e^{\delta x}u\,dx = {}_2F_1[1, 1+\delta, 2+\delta, -e^x]e^{(1+\delta)x}/(1+\delta)$. Some software platforms, including Python and Mathematica, have a built-in calculation of the hypergeometric function ${}_2F_1$. Using Mathematica, this analytic solution exceeds the result from the Euler method described below by an average of 0.23% and maximum of 0.27% times the year 1750 value for <N_2O> and by a mean of 0.08% and a maximum of 0.16% times the year 1750 value for <CH_4>.

Absent a hypergeometric function evaluator, another approach starts by re-writing equation (3.3) as

$$g_i = rg_{i-1} + a_1(u_{i-1} - u_0) \tag{A.6}$$

where $g_i = G_i - G_0$ and $r = (1 - 1/t_G)$. Then $g_1 = 0$, $g_2 = S_1$, $g_3 = rg_2 + S_2 = rS_1 + S_2$, $g_4 = rg_3 + S_3 = r^2S_1 + rS_2 + S_3$, and in general $g_{i+1} = \sum_{j=0}^{i-1} r^j S_{i-j}$. This treats the solution as the sum of the results of a series of short emission pulses. This is an example of a discrete Green's function solution method. Since $S_{i-j} = a_1u_{i-j} - a_1u_0$ and a geometric series sums to $\sum_{j=0}^{i-1} r^j = (1 - r^{i-1})/(1 - r)$, the number of operations needed to compute g_{i+1} is reduced by writing the answer as

$$g_{i+1} = (a_1 \sum_{j=0}^{i-1} r^j u_{i-j}) - a_1u_0(1 - r^{i-1})/(1 - r) \tag{A.7}$$

References

[1] Singer, C. and L. Matchett, 2015. Climate Action Gaming Experiment: Methods and example Results, *Challenges* **6**. 202–228, https://doi.org/10.3390/challe6020202.

[2] Chen, N. 2021. Conformity and confirmation: group decision-making in foreign policy. University of Illinois at Urbana-Champaign PhD Thesis, https://www.ideals.illinois.edu/handle/2142/110701.

[3] Ding, C., and C. Singer. 2022. University of Illinois at Urbana-Champaign Program in Arms Control & Domestic and International Security Research Reports ACDIS//ACDIS DIN:1, Climate Action Game Experiment motivation and role of radiative forcing; DIN:2, Calibration and extrapolation of a simple global carbon balance model; DIN:3, Non-anthropogenic influences on global average temperature; DIN:4, Global heat balance model parameters; DIN:5, Extrapolations of global average temperature, sea level rise, and ocean pH change; DIN:6, Global heat balance equation probability distributions and extrapolations; https://acdis.illinois.edu/outreach/research/research-reports.

[4] Yang, B. 2021. Economic analysis of international climate cooperation. University of Illinois at Urbana-Champaign PhD Thesis, https://www.ideals.illinois.edu/handle/2142/110488.

[5] MacDougall, A. H., T. L. Frölicher, C. D. Jones, J. Rogelj, H. D. Matthews, K. Zickfeld, V. K. Arora, N. J. Barrett, V. Brovkin, F. A. Burger, M. Eby, A.V. Eliseev, T. Hajima, P. B. Holden, A. Jeltsch-Thömmes, C. Koven, N. Mengis, L. Menviel, M. Michou, I. I. Mokhov. A. Oka, J. Schwinger, R. Séférian, G. Shaffer, A. Sokolov, K. Tachiiri, J. Tjiputra, A. Wiltshire, and T. Ziehn. 2020. Is there warming in the pipeline? A multi-model analysis of the Zero Emissions Commitment from CO_2. *Biogeosciences*, **17**, 2987–3016, https://doi.org/10.5194/bg-17-2987-2020.

[6] Butler, J. H., and S. A. Montzka. 2017. The NOAA annual greenhouse gas index (AGGI), https://www.esrl.noaa.gov/gmd/aggi/aggi.html, accessed 6 December 2020.

[7] Wigley, T. M. L., C. Ammann, B. D. Santer, and S. C. B. Raper. 2005. Effect of climate sensitivity on the response to volcanic forcing, em Climate and Dynamics **10**, Issue D9, https://doi.org/10.1029/2004JD005557.

[8] Knutti, R. and A. A. Rugenstein. 2015. Feedbacks, climate sensitivity and the limits of linear models, Philosophical Transactions of the Royal Society A. **373** 20150146, http://doi.org/10.1098/rsta.2015.0146.

[9] Bloch-Johnson, J., R. T. Pierrehumbert, and D. S. Abbot. 2015. Feedback temperature dependence determines the risk of high warming, *Geophysical Research Letters* **42**, 4973-4980, https://doi.org/10.1002/2015GL064240.

[10] IPCC, 2021. *Climate Change 2021: The Physical Science Basis. Contribution of Working Group I to the Sixth Assessment Report of the Intergovernmental Panel on Climate Change*, V. Masson-Delmotte, P. Zhai, A. Pirani, S. L. Connors, C. Pèan, S. Berger, N. Caud, Y. Chen, L. Goldfarb, M. I. Gomis, M. Huang, K. Leitzell, E. Lonnoy, J. B. R. Matthews, T. K. Maycock, T. Waterfield, O. Yelekçi, R. Yu and B. Zhou (eds.). Cambridge University Press. In Press, https://www.ipcc.ch/report/sixth-assessment-report-working-group-i/.

[11] Miller, R. L., G. A. Schmidt, L. S. Nazarenko, N. Tausnev, S. E. Bauer, A. D. DelGenio, M. Kelley, K. K. Lo, R. Ruedy, D. T. Shindell, I. Aleinov, M. Bauer, R. Bleck, V. Canuto, Y. Chen, Y. Cheng, T. L. Clune, G. Faluvegi, J. E. Hansen, R. J. Healy, N. Y. Kiang, D. Koch, A. A. Lacis, A. N. LeGrande, J. Lerner, S. Menon, V. Oinas, C. P. García-Pando, J. P. Perlwitz, M. J. Puma, D. Rind, A. Romanou, G. L. Russell, M. Sato, S. Sun, K. Tsigaridis, N. Unger, A. Voulgarakis, M.-S. Yao, and J. Zhang. 2014. CMIP5 historical simulations (1850-2012) with GISS ModelE2, *Journal of Advances in Modeling of Earth Systems* **6**, no. 2441-2477, https://doi.org/10.1002/2013MS000266.

[12] Etheridge, D. M. et al. 2010. Law Dome Ice Core 2000-Year CO2, CH4, and N2O Data. IGBP PAGES/World Data Center for Paleoclimatology Data Contribution Series # 2010-070. NOAA/NCDC Paleoclimatology Program, Boulder CO, USA, ftp://ftp.ncdc.noaa.gov/pub/data/paleo/icecore/antarctica/law/law2006.txt, and references therein, including Etheridge, D. M., L. P. Steele, R. L. Langenfelds, R. J. Francey, J.-M. Barnola, and V. I. Morgan. 1996. Natural and anthropogenic changes in atmospheric CO2 over the last 1000 years from air in Antarctic ice and firn, *Journal of Geophysical Research*, **101**, 4115–4128, https://doi.org/10.1029/95JD03410.

[13] Etheridge, D., L. Steele, R. Langenfelds, R. Francey, J. Barnola, and V. Morgan. 1998. Historical CO_2 records from the Law Dome DE08, DE08-2, and DSS ice cores. In Trends: A Compendium of Data on Global Change. Carbon Dioxide Information Analysis Center, Oak Ridge National Laboratory, U.S. Department of Energy, Oak Ridge, TN, USA, https://cdiac.ess-dive.lbl.gov/trends/co2/lawdome.html, accessed August 29, 2021.

[14] Lee, D. S., D. W. Fahey, A. Skowron, M. R. Allen, U. Burkhardt, Q. Chen, S. J. Doherty, S. Freeman, P. M. Forster J. Fuglestvedt, A. Gettelman, R. R. De León, L. L. Lim, M. T. Lund, R. J. Millar, B. Owen, J. E. Penner, G. Pitari, M. J. Prather, R. Sausen, and L. J. Wilcox. 2020. The contribution of global aviation to anthropogenic climate forcing for 2000 to 2018. *Atmospheric Environment*, **244**, 117834, https://doi.org/10.1016/j.atmosenv.2020.117834.

[15] IPCC. 2013. *Climate Change 2013: The Physical Science Basis. Contribution of Working Group I to the Fifth Assessment Report of the Intergovernmental Panel on Climate Change*, T. Stocker, D. Qin, G.-K. Plattner,

M. Tignor, S. Allen, J. Boschung, A. Nauels, Y. Xia, V. Bex and P. Midgley (eds.), Cambridge University Press, Cambridge, United Kingdom and New York, NY, USA, https://www.ipcc.ch/report/ar5/wg1/.

[16] Smith, C., G. Harris, M. Palmer, N. Bellouin, W. Collins, G. Myhre, M. Schulz, J.-C. Golaz, M. Ringer, T. Storelvmo, and P. Forster. 2021. Energy budget constraints on the time history of aerosol forcing and climate sensitivity, *JGR Atmospheres*, **126**, No. 13, https://doi.org/10.1029/2020JD033622.

[17] Deng, J., A. Dai, and H. Xu. 2020. Nonlinear climate response to increasing CO_2 and anthropogenic aerosols simulated by CESM1, *Journal of Climate* **33**, 281-301, https://doi.org/10.1175/JCLI-D-19-0195.1.